

Original Article



Comprehensive Lipid Profiling Recapitulates Enhanced Lipolysis and Fatty Acid Metabolism in Intimal Foamy Macrophages From Murine Atherosclerotic Aorta

Jae Won Seo ^{1,†}, Kyu Seong Park ^{2,†}, Gwang Bin Lee ¹, Sang-eun Park ²,
Jae-Hoon Choi ^{2,*}, Myeong Hee Moon ^{1,*}

OPEN ACCESS

Received: Feb 20, 2023
Revised: May 9, 2023
Accepted: May 21, 2023
Published online: Jun 15, 2023

*Correspondence to

Jae-Hoon Choi

Department of Life Science, Research Institute for Natural Sciences, Hanyang Institute of Bioscience and Biotechnology, College of Natural Sciences, Hanyang University, 222 Wangsimni-ro, Seongdong-gu, Seoul 04763, Korea.
Email: jchoi75@hanyang.ac.kr

Myeong Hee Moon

Department of Chemistry, Yonsei University, 50 Yonsei-ro, Seodaemun-gu, Seoul 03722, Korea.
Email: mhmoon@yonsei.ac.kr

[†]Jae Won Seo and Kyu Seong Park contributed equally to this work.

Copyright © 2023. The Korean Association of Immunologists

This is an Open Access article distributed under the terms of the Creative Commons Attribution Non-Commercial License (<https://creativecommons.org/licenses/by-nc/4.0/>) which permits unrestricted non-commercial use, distribution, and reproduction in any medium, provided the original work is properly cited.

ORCID iDs

Jae Won Seo
<https://orcid.org/0000-0001-6794-897X>
Kyu Seong Park
<https://orcid.org/0000-0002-5016-6995>
Gwang Bin Lee
<https://orcid.org/0000-0003-4756-0921>

¹Department of Chemistry, Yonsei University, Seoul 03722, Korea

²Department of Life Science, Research Institute for Natural Sciences, Hanyang Institute of Bioscience and Biotechnology, College of Natural Sciences, Hanyang University, Seoul 04763, Korea


ABSTRACT

Lipid accumulation in macrophages is a prominent phenomenon observed in atherosclerosis. Previously, intimal foamy macrophages (FM) showed decreased inflammatory gene expression compared to intimal non-foamy macrophages (NFM). Since reprogramming of lipid metabolism in macrophages affects immunological functions, lipid profiling of intimal macrophages appears to be important for understanding the phenotypic changes of macrophages in atherosclerotic lesions. While lipidomic analysis has been performed in atherosclerotic aortic tissues and cultured macrophages, direct lipid profiling has not been performed in primary aortic macrophages from atherosclerotic aortas. We utilized nanoflow ultrahigh-performance liquid chromatography-tandem mass spectrometry to provide comprehensive lipid profiles of intimal non-foamy and foamy macrophages and adventitial macrophages from *Ldlr*^{-/-} mouse aortas. We also analyzed the gene expression of each macrophage type related to lipid metabolism. FM showed increased levels of fatty acids, cholesterol esters, phosphatidylcholine, lysophosphatidylcholine, phosphatidylinositol, and sphingomyelin. However, phosphatidylethanolamine, phosphatidic acid, and ceramide levels were decreased in FM compared to those in NFM. Interestingly, FM showed decreased triacylglycerol (TG) levels. Expressions of lipolysis-related genes including *Pnpla2* and *Lpl* were markedly increased but expressions of *Lpin2* and *Dgat1* related to TG synthesis were decreased in FM. Analysis of transcriptome and lipidome data revealed differences in the regulation of each lipid metabolic pathway in aortic macrophages. These comprehensive lipidomic data could clarify the phenotypes of macrophages in the atherosclerotic aorta.


Keywords: Atherosclerosis; Macrophages; Hyperlipidemic mice; Lipidomics; nUHPLC-ESI-MS/MS

INTRODUCTION

Atherosclerosis is a major chronic inflammatory cardiovascular disease that leads to heart attack, myocardial infarction, and ischemic stroke (1). The low-density lipoprotein (LDL)

Sang-eun Park 

<https://orcid.org/0000-0001-9766-9832>

Jae-Hoon Choi 

<https://orcid.org/0000-0002-5265-3463>

Myeong Hee Moon 

<https://orcid.org/0000-0002-5454-2601>

Conflict of Interest

The authors declare no potential conflicts of interest.

Abbreviations

AA, arachidonic acid; AM, Adventitial macrophages; CPM, control group of peritoneal macrophages; CE, cholesteryl ester; Cer, ceramide; ER, endoplasmic reticulum; FM, intimal foamy macrophages; FA, fatty acid; FAO, fatty acid oxidation; GP, glycerophospholipid; HFA, hydroxylated fatty acid; IS, internal standards; LcTG, longer acyl chains; LDL, low-density lipoprotein; LPA, lysophosphatidic acid; LPC, lysophosphatidylcholine; NFM, intimal non-foamy macrophages; nUHPLC-ESI-MS/MS, nanoflow ultrahigh-performance liquid chromatography-electrospray ionization-tandem mass spectrometry; OPM, oxLDL-treated peritoneal macrophages; PC, phosphatidylcholine; PE, phosphatidylethanolamine; PI, phosphatidylinositol; PL, phospholipid; PPAR, peroxisome proliferator-activated receptors; PS, phosphatidylserine; SctG, shorter acyl chains; SM, sphingomyelin; TG, triacylglycerol or triglyceride.

Author Contributions

Conceptualization: Seo JW, Park KS, Choi JH, Moon MH; Data curation: Seo JW, Park KS; Formal analysis: Seo JW, Park KS; Funding acquisition: Choi JH, Moon MH; Investigation: Seo JW, Park KS, Lee GB, Park SE; Resources: Park SE; Supervision: Choi JH, Moon MH; Visualization: Seo JW, Park KS; Writing - original draft: Seo JW, Park KS; Writing - review & editing: Choi JH, Moon MH.

particles that accumulate on the arterial wall due to hyperlipidemia are vulnerable to oxidative modification, triggering inflammatory processes, including the accumulation of monocytes/macrophages in the subintimal space (2). These accumulating macrophages play essential roles in the progression and regression of atherosclerosis via the production of inflammatory cytokines, clearance of dead cells, antigen presentation, and lipid uptake or efflux (3). It is well-known that the development of atherosclerotic plaque is associated with the formation of macrophage foam cells with excessive cellular lipid accumulation (4).

Lipids are the main components of cellular membranes and are classified into 8 different categories: glycerophospholipids (GPs), glycerolipids, sphingolipids, sterols, fatty acids (FAs), prenols, saccharolipids, and polyketides (5). Lipids not only structure the membrane of cells, but play important roles in energy storage, signal transduction, cell growth, apoptosis, etc. (6,7). Alterations of lipid profiles are significantly associated with the development of various metabolic diseases including atherosclerosis, obesity, diabetes, and cancer (8-11). Lipid metabolism has also been known to control the phenotype of macrophages (12). A transcriptome analysis of intimal foamy macrophages (FM) and intimal non-foamy macrophages (NFM) found that foamy macrophages have enhanced lipid metabolic pathway including cholesterol uptake, efflux, and processing related genes, but attenuated inflammatory pathway compared to non-foamy macrophages (13). These results strongly suggest that the lipid accumulation in macrophages can reprogram the lipid metabolism leading to alteration of immunological function during atherosclerosis. Therefore, it is important to analyze the lipid composition of macrophages to understand the exact lipid metabolism in macrophages during atherosclerotic processes. Recently, lipidome analysis showed that the levels of phosphatidylinositol (PI), phosphatidylglycerol, and phosphatidylserine (PS) were increased in M1-like macrophages; however, the levels of lysoglycerophospholipids were increased in M2-like macrophages (14). Moreover, the lipid composition of macrophages can be differently altered upon stimulation with each TLR, and these compositional changes of cellular lipids have an important role in the inflammatory response of macrophage (15). Although previous studies have analyzed the lipids targeting atherosclerosis using cultured mouse and human macrophages (14), human atherosclerotic plaques (8), and oxLDL treated in vitro foam cells (16), a comprehensive lipid profiling of intimal macrophages is important to understand macrophage lipid metabolism during atherosclerosis since the tissue microenvironment can affect the metabolic phenotype of macrophages. However, a detailed lipidomic analysis of intimal macrophages has not been accomplished due to the difficulty in obtaining sufficient cells for lipid analysis.

In this study, 3 types of macrophages including FM, NFM, and adventitial macrophages (AM), were isolated from atherosclerotic mouse aortas using a flow cytometric approach with fluorescence lipid staining (13) and their lipid profiles were analyzed using nanoflow ultrahigh-performance liquid chromatography-electrospray ionization-tandem mass spectrometry (nUHPLC-ESI-MS/MS). Lipid analysis of the 3 macrophages was performed with non-targeted identification of lipid molecular structures based on data-dependent collision-induced dissociation, followed by high-speed targeted quantification using the full MS scanning method. To understand the characteristics of intimal foamy and non-foamy macrophages, alterations in their lipid profiles (in comparison to AM) have been investigated at the levels of lipid classes and individual lipid species. In addition, transcriptomic analyses related to lipid metabolism pathways were performed to provide evidence and enable a deeper understanding of the lipidomic outcomes.

MATERIALS AND METHODS

Detailed experimental procedures of lipidomic analysis can be found in the **Supplementary Data 1**.

Mouse and peritoneal cells

Ldlr^{-/-} mice (C57BL/6/J background) were obtained from Jackson Laboratory (Bar Harbor, ME, USA) and maintained under specific pathogen-free conditions. To induce atherosclerosis, 8-week-old male *Ldlr*^{-/-} mice were fed a western diet for 16 wk. Western diet (49.9% carbohydrates, 19.8% protein, 21% fat, and 0.15% cholesterol) was purchased from a local vendor (D12079B; Research Diets, New Brunswick, NJ, USA). To achieve an appropriate single-cell number, 39 mice were sacrificed. For *in vitro* test, male C57BL/6 mice (n=7) were injected intraperitoneally with 1 ml of 3% thioglycolate broth medium. 3 days later, peritoneal macrophages were isolated with 5 ml of RPMI1640 containing 10% FBS. The cells were cultured in 6 well plate for 3 h to wash away with PBS and then incubated in the incubator at 37°C with 5% CO₂. After overnight incubation, commercial oxidized LDL (20 µg/ml; cat.770202; Kalen Biomedical, Montgomery Village, MD, USA) were treated to the cells for 48 h. All animal procedures were approved by the local authorities and Institutional Animal Care and Use Committee of Hanyang University, Seoul (permission number: 2020-0120A), and performed in accordance with the relevant guidelines and regulations. The study complied with Animal Research: Reporting of *In Vivo* Experiments guidelines.

Aortic intimal and adventitial singlet preparation

Mice were euthanized with a CO₂ which fill rate of 30%–50% of the chamber volume per minute and perfused via the left cardiac ventricle with approximately 10 ml of fresh cold PBS to eliminate blood contamination before isolating the aorta. The entire aorta (including the aortic sinus, arch, thoracic aorta, and abdominal aorta) was carefully dissected, and the perivascular fat and cardiac muscle were removed. Single-cell suspensions of the aorta were prepared as previously described (13). In brief, isolated aortas were opened longitudinally and washed again with PBS. The total aortic tissue was incubated at 37°C for 8 min with gentle rotation in a PBS solution containing calcium, magnesium, collagenase II (400 U/ml; cat. C6885; Sigma Aldrich, St. Louis, MO, USA), and hyaluronidase (90 U/ml) to separate the intima-media layer from the adventitia. After physically separating the aortic layers, the aortic intima and adventitia were digested in a PBS solution containing calcium, magnesium, collagenase I (675 U/ml), collagenase XI (187.5 U/ml), DNase I (90 U/ml), and hyaluronidase (90 U/ml), at 37°C for 60 min and 20 min, respectively, with rotation. After digestion, the intimal and adventitial cells were filtered through a 70 µm cell strainer and centrifuged at 385 × g for 7 min at 4 °C and resuspended in 2% FBS in PBS to obtain single cell suspensions. To load an adequate number of cells into the flow cytometer, the cell number was counted using a hemocytometer, and the cell suspensions were aliquoted into tubes for FACS. To distinguish dead cells, the cells were pre-stained with propidium iodide solution just before loading the cells into the flow cytometer according to the manufacturer's instructions.

Isolation of aortic macrophages

The Fc receptor was blocked to prevent non-specific binding by TruStain FcX antibody (clone 93; cat.101319) for 15 min at 4°C and the cells were incubated with the antibody mixture at 4°C for 30 min. The antibody mixture included the CD45 (clone 30-F11; cat.103113), CD11b (clone M1/70; cat. 101241), and CD64 (clone X54-5/7.1; cat. 139307). The cells were gently washed with 2% FBS in PBS and incubated with 40 nmol/l BODIPY493/503 (cat. D3922; Invitrogen,

Waltham, MA, USA) in PBS at 4 °C for 30 min. The stock solution (10 mmol/l BODIPY493/503 in DMSO) was diluted with PBS in a 1:400 ratio. Three different types of aortic macrophages were sorted from atherosclerotic aortas from *Ldlr^{-/-}* mice (n=39) using a BD FACS Aria III Cell Sorter (BD Life Sciences, San Jose, CA, USA). The number of macrophages used for lipid extraction was approximately 50,000 cells for both AM and NFM, and 45,000 cells for FM. Macrophage samples were stored at -80°C until lipid extraction.

Oil Red O staining of sorted aortic macrophages

Sorted aortic macrophages were placed on positively charged slide glasses and fixed with 4% paraformaldehyde for 30 min. After washing with distilled water, 100% propylene glycol was added to the slides and incubate for 2 min. And then the macrophages were stained with Oil Red O working solution for 15 min and were rinsed with 60% propylene glycol and distilled water sequentially. Finally, the stained macrophages were covered with aqueous mounting medium and observed under light microscope.

Lipid analysis

A fused silica capillary tube with an inner diameter of 100 µm and outer diameter of 360 µm from Polymicro Technology, LLC (Phoenix, AZ, USA) was used to prepare the capillary columns. Watchers® ODS-P C-18 particles (3 µm and 100 Å) from Isu Industry Corp. (Seoul, Korea) and BEH Shield C18 particles (1.7 µm and 130 Å), unpacked from an ACQUITY UPLC BEH Shield RP18 column (2.1 mm × 100 mm) purchased from Waters (Milford, MA, USA), were used as packing materials for capillary columns.

Lipid extraction

A mixture of internal standards (IS) was added to each group of samples prior to lipid extraction for lipid quantitation. For lipid extraction, each group of samples was tip sonicated for 2 min, and 1,300 µl of MeOH/MTBE/CHCl₃ mixture (1.33:1:1, v/v/v) was added to each group. The mixture was vortexed for 10 min at 40°C and then centrifuged at 1,000 × g for 10 min. The resulting organic layer was transferred to a different Eppendorf tube and dried under N₂ gas using an Evatros mini evaporator (Goojung Engineering, Seoul, Korea). Dried lipid extracts were dissolved in 150 µl of MeOH/CHCl₃/H₂O (18:1:1, v/v/v) for both AM and NFM and 135 µl for foamy macrophages to obtain the same concentration for all groups. Each sample was stored at -80°C until nUHPLC-ESI-MS/MS analysis. Details of lipid analysis by nUHPLC-ESI-MS/MS are described in **Supplementary Data 1**.

Lipid and nUHPLC-ESI-MS/MS analysis

A mixture of IS was added to each group of samples prior to lipid extraction for lipid quantitation. Fifty lipid standards were purchased from Avanti Polar Lipids Inc. (Alabaster, AL, USA) and listed in Supplementary information. Qualitative and quantitative lipid analyses were carried out using a Dionex Ultimate 3000 RSLCnano System coupled with Q Exactive Orbitrap MS from Thermo Fisher Scientific (San Jose, CA, USA). Details of nUHPLC-ESI-MS/MS run conditions are also in **Supplementary Data 1**.

Bulk RNA-sequencing analysis

We reanalyzed our previous bulk RNA-sequencing data (13) of intimal foamy, non-foamy and AM. The sequencing data is used for listing up the significant lipid metabolic pathways and related genes: FA biosynthesis and β-oxidation; triacylglycerol (TG) biosynthetic and catabolic pathways; cholesterol esterification; GP biosynthesis; and sphingomyelin (SM) and ceramide (Cer) conversion. To confirm the substantial number of genes, box plots were

used to represent differentially expressed genes between intimal foamy and non-foamy macrophages (fold ratio ≥ 1.5 , $p < 0.05$). Data was analyzed by ROSALIND® (<https://rosalind.bio/>), with a HyperScale architecture developed by ROSALIND, Inc. (San Diego, CA, USA). Reads were trimmed using cutadapt (17). Quality scores were assessed using FastQC (FastQC: a quality control tool for high throughput sequence data, Andrews S., 2010). Reads were aligned to the *Mus musculus* genome build mm10 using STAR (18). Individual sample reads were quantified using HTseq (19) and normalized via Relative Log Expression using DESeq2 R library (20). Read Distribution percentages, violin plots, identity heatmaps, and sample MDS plots were generated as part of the QC step using RSeQC (21). DESeq2 was also used to calculate fold changes and p-values and perform optional covariate correction.

Data availability

Bulk RNA sequencing datasets are available in the international public repository, Gene Expression Omnibus, under accession identification as GSE116239 (13).

RESULTS

Targeted quantification of lipids in aortic macrophages from atherosclerosis-induced mice

To investigate the role of lipid metabolism in aortic macrophages in atherosclerosis, we isolated 3 types of macrophages from the aorta of high-fat diet-fed *Ldlr*^{-/-} mice ($n=39$). The AM (CD45⁺CD11b⁺CD64⁺BODIPY^{low}SSC^{low}, cell number=50,000), FM (CD45⁺CD11b⁺CD64⁺BODIPY^{high}SSC^{high}, cell number=45,000), and NFM (CD45⁺CD11b⁺CD64⁺BODIPY^{low}SSC^{low} cell number=50,000) were sorted out using lipid probe-based flow cytometry (Fig. 1A). The sorted FM had abundant cytoplasm with Oil Red O-positive lipid droplets, whereas other cells did not (Fig. 1B). Lipid extracts of each macrophage were analyzed by nUHPLC-ESI-MS/MS under run conditions that were optimized in both positive and negative ion modes using a mixture of lipid standards (Supplementary Fig. 1). The base peak chromatograms of the lipid extract sample (AM, NFM, and FM) are shown in Supplementary Fig. 2. A total of 557 lipids from 21 lipid classes were identified with their molecular structures from data-dependent MS/MS experiments, of which 218 species were quantified because the targeted quantification was based on lipids with different numbers of total carbon and double bonds (Supplementary Table 1). The identified chain structures of each quantified species are presented in Supplementary Table 2. Owing to the use of a limited number (45,000 cells for FM) of macrophages, it was not possible to determine the absolute concentrations of individual lipids based on calibration, which requires sufficient amount of lipid extracts to prepare a series of standard solutions with varying concentrations of external standards. Instead, quantification of lipids was carried out with the pooled macrophages for each group by comparing the corrected peak area, which was the relative peak area of an individual lipid species, to the peak area of an IS inserted into each lipid class. Therefore, it was focused to compare the relative profile of lipids within each lipid class between FM and NFM groups in comparison to that of AM. Supplementary Table 3 shows the calculated fold ratio of each lipid species in the NFM group compared to the AM group (hereinafter referred to as NFM/AM), FM/AM, and FM/NFM together with that in *in vitro* oxLDL-treated peritoneal macrophages (OPM) compared to control peritoneal macrophages (CPM).

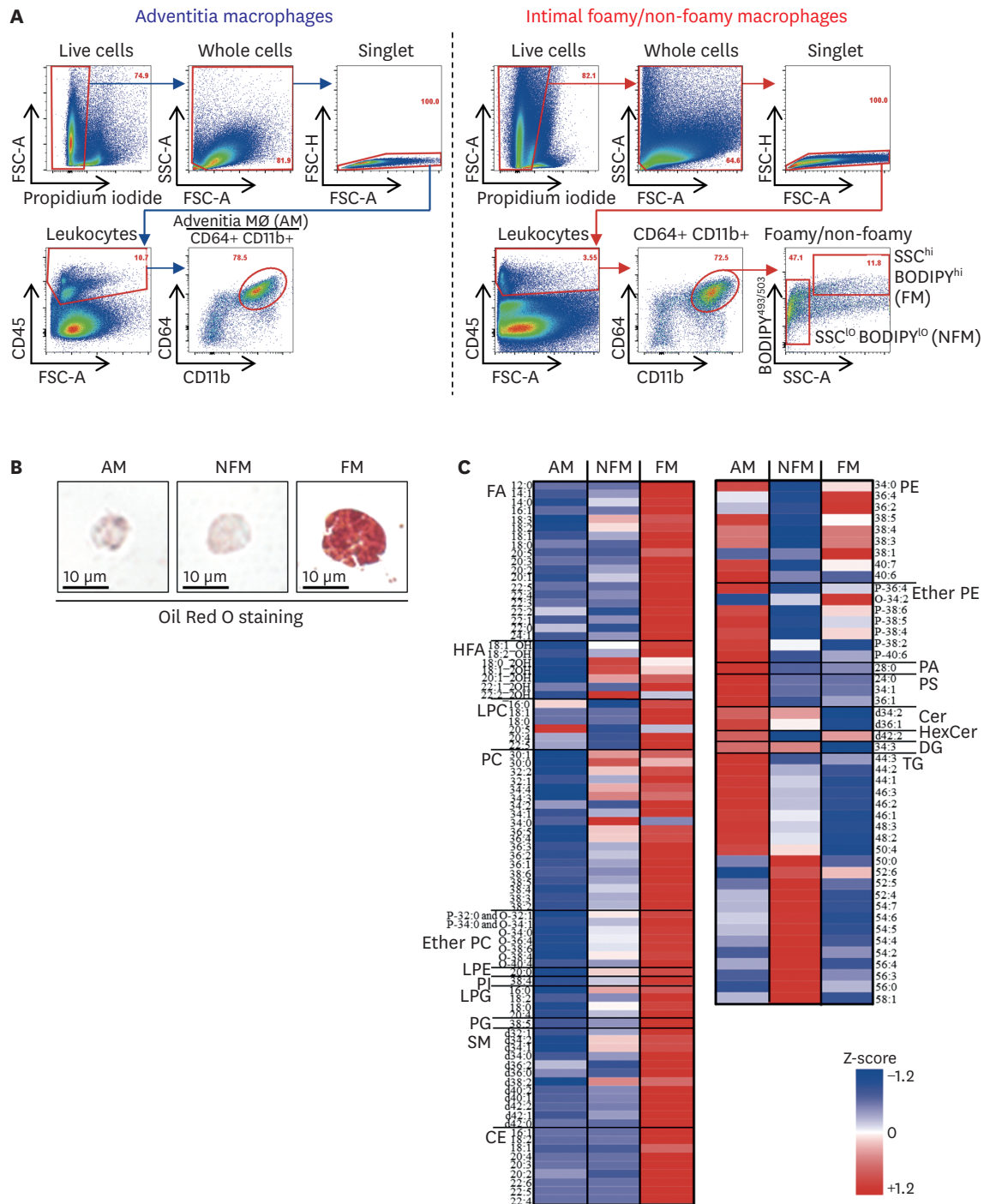


Figure 1. Distinct lipid profiles of aortic macrophages from hyperlipidemic mice. (A) FACS sorting strategy for aortic macrophages. *Ldlr*^{-/-} mice (n=39) fed with HFD for 16 wk to induce atherosclerosis. Live AM (propidium iodide CD45⁺CD64⁺CD11b⁺), FM (SSC^{hi}BODIPY^{hi}) and NFM (SSC^{lo}BODIPY^{lo}) were sorted from atherosclerosis aortas. Cells were obtained from approximately 5.0×10⁴ AM cells, 4.5×10⁴ FM cells and 5.0×10⁴ NFM cells, respectively. (B) Morphology of aortic macrophages. Cells were sorted from atherosclerotic aorta of *Ldlr*^{-/-} mice (n=2), stained with Oil Red O, and analyzed by optical electron microscopy. (C) Heat map of lipid species showing >2-fold changes in NFM (vs. AM) or FM (vs. NFM or AM). HFD, high fat diet; FSC-A, forward scatter area; FSC-H, forward scatter height; SSC-A, side scatter area; LPE, lysophosphatidylethanolamine; DG, diacylglycerol.

Distinct cellular lipid profiles among 3 aortic macrophage populations

From the quantified results of 218 lipid species, the differences in lipid levels can be visualized with a heat map, which was plotted with lipid species showing >2-fold changes in

at least one of the 3 comparisons (NFM vs. AM, FM vs. AM, and FM vs. NFM) (**Fig. 1C**). Levels of lipid classes such as FA, phosphatidylcholine (PC) including lysophosphatidylcholine (LPC) and etherPC, SM, and cholesteryl esters (CEs) were found to be increased in FM compared to those in both AM and NFM, as sorted in the left part of the heat map; however, levels of ether phosphatidylethanolamine (PE), PS, Cer, and TG were decreased in FM sorted on the right side. While most lipid classes in the right column of the heat map showed the highest levels in AM, levels of TG showed significant differences depending on their chain lengths, with long chain structures (total carbon number >50) increasing in the NFM group and decreasing in the FM group. For the visual demonstration of relative changes in amounts with heat map, variance of each individual species level was used with that of 5 repeated measurements.

TG and FAs levels of 3 aortic macrophage populations

Changes in individual TG levels are plotted in **Fig. 2A** with the relative fold ratio of individual TG species in FM vs. AM and NFM vs. AM. Levels of TG with shorter acyl chains (total carbon number <50, hereafter, ScTG) exhibited a decreasing pattern from AM to NFM and FM; however, those with longer acyl chains (total carbon number >50, hereafter as LcTG) appeared with an increased pattern in NFM (vs. AM) but a decreased pattern in FM. This suggests that ScTG species did not accumulate in either of the intimal cells, whereas LcTG species accumulated in NFM to a greater extent than in FM, and their accumulation was largely reduced in FM.

The overall FA level as shown in **Fig. 2B** was increased about 2-folds in FM, compared to those of the other 2 groups. FA levels were expressed as the corrected peak area, which is the peak area of each species relative to that of the IS of each lipid class. The amounts of individual lipid species in each lipid class in **Fig. 2B** are visualized with stacked bar graphs, and the relative levels of each lipid class were compared between the different macrophage types. Lipid species provided with acyl chain information on the right side of each bar in **Fig. 2B** belongs to the highly abundant species in each class, and “low” refers to the summation of peak area of the rest of lipid species. Highly abundant species were defined as the lipid species with which the abundance was higher than 100%/(number of lipid species in each class). The concentration of each IS is listed in **Supplementary Table 4**. In the case of detecting FAs from plastics or extraction solvents that could interfere with FA analysis, background correction was applied to calculate endogenous FA signals and the concentrations of FAs in the blank sample are listed in **Supplementary Table 5**. The overall levels of hydroxylated fatty acids (HFAs) in both intimal macrophages were similar to each other but largely different from that in AM, showing a large contrast between intimal macrophages and AM. It is noted that the relative ratio of HFA 18:1_OH to HFA 22:1_OH is reversed in both FM and NFM groups. Individual FA levels in the 3 macrophages are plotted in **Fig. 2C**, together with the total levels of ScTG, LcTG, and HFA. The TG molecular types of each FA are listed in **Supplementary Table 6**. FA 18:1 level was higher in FM by 3.8-fold than in NFM, whereas it was not detected in AM. However, the level of TG species containing 18:1 acyl chain was lowest in the FM group for both ScTG and LcTG groups. A similar pattern was observed for FA 18:2. In both cases, LcTG levels were elevated in NFM. A similar observation was made for long FAs (20:3, 22:5, and 22:3), which were not detected in either the AM or NFM groups, but their LcTG levels were higher in the NFM group than in the FM group. In the case of HFA, FA 18:1_OH and FA 18:0_2OH, both hydroxylated forms of FA 18:2, showed opposite trends in their levels in the NFM and FM groups, with the monohydroxyl form of FA 18:2 being higher in the FM group, whereas the dihydroxyl form was lower in FM than in NFM. A similar trend was observed for FA 18:3 (**Supplementary Fig. 3**), where the remaining plots of FA species (FA 12:0, 18:3, 20:2, 20:5, and 22:2) are displayed. These results imply that

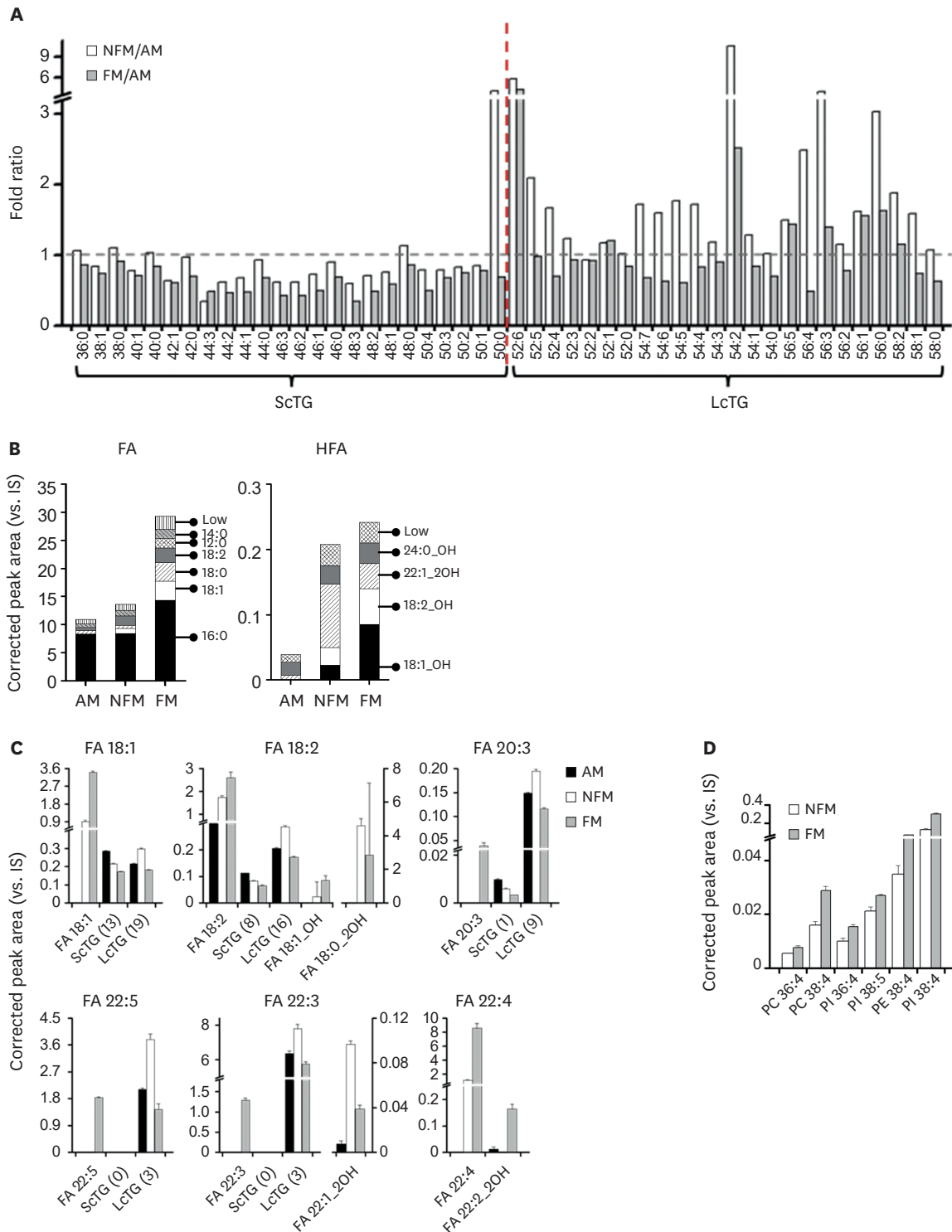


Figure 2. Decreased TG level but increased FAs in FM. The analysis was repeated 5 times in polarity switching mode for quantification with the amount of lipid extract equivalent to 200 cells injected per each run. (A) Fold ratio of TG species in NFM and FM macrophages with respect to those of AM. Vertical dashed line refers to the point of total carbon number 50. SctTG indicates TG group with short chains, and LctTG is for TG group with long chains. (B) The cellular levels of FA and HFA (relative to IS) compared between each macrophage group. High abundance lipid species in each class are represented with acyl chain information and the “low” represents the summed amount of all low abundance species. (C) Corrected peak areas of 6 FA showing significant differences in FM (vs. NFM) compared with those of TG species containing each corresponding fatty acyl chains along with their oxidized products (HFA). (D) Comparison of PLs containing arachidonoyl (20:4) acyl chain between the FM and NFM. SctTG and LctTG refer to TG groups with total carbon number below 50 and above 50, respectively. Numbers inside the parentheses refers to the counted number of TG species in each short chain and long chain TG groups.

decreased TG levels are associated with the release of FA from TG through lipolysis and fatty acid oxidation (FAO) to produce ATP in mitochondria (22).

Arachidonic acid (AA or FA 20:4) is a precursor of eicosanoids that are known to have proinflammatory and immunoregulatory roles (23). In particular, PI 38:4 (or PI 18:0/20:4) has been reported as a highly abundant PI species that controls the inflammation process and is a major source of AA (24). While free AA was not detected from macrophages in this study, phospholipids (PLs) containing arachidonoyl acyl chains were examined, since AA is released from PLs by phospholipase A2 and is the precursor of lipoxin A4 and PGE2, which are involved in the activation of macrophages (25,26). **Fig. 2D** shows the comparison of the relative amounts of 6 PLs containing an arachidonoyl chain between the FM and NFM, with the levels of all 6 PL species higher in the FM than in the NFM. Interestingly, PLs with an 18:0/20:4 acyl chain, corresponding to PC 38:4, PE 38:4, and PI 38:4, were more accumulated in the FM group by about 2-fold compared to those in the NFM.

Differential expression of genes related to metabolic process of FA and TG

To validate the genes that contribute to the TG and FA metabolic processes, which is a characteristic of FM, we analyzed the previously performed bulk RNA-sequencing data (13). The pathways of FA biosynthesis, FA beta-oxidation, and biosynthesis and lysis of TG were primarily investigated because the products of FA biosynthesis are used as the source of FA beta-oxidation, and their products are associated with TG synthesis (22). Lysis of TG also positively regulates the FA synthesis. The pathways are represented in a schematic diagram and the genes regulating each process are indicated in **Supplementary Fig. 4**. According to previous research, *Elovl5* and *Scd5* are involved in the FA biosynthetic process (27) and produce acyl-coenzyme A. RNA-seq data showed that *Elovl1*, *Scd1*, and *Scd2* were upregulated in FM (**Fig. 3A**). Palmitoyl-CoA, produced by the FA synthesis process, is oxidized by multiple genes, such as *Echs1*, *Hadh*, and *Acads* (27). The RNA levels of these genes are higher in FM than in NFM (**Fig. 3B**), which coincide with the lipidomic results. *Agpat1* and *Agpat3* increased in FM to enhance the transformation of lysophosphatidic acid (LPA) to phosphatidic acid (**Fig. 3C**). *Lpin2* and *Dgat1*, associated with TG synthesis (28) are decreased whereas *Pnpla2* and *Lpl*, which are related in lipolysis of TG (29,30), are increased in FM (**Fig. 3C**). These results can explain why the TG level was lower in FM than in AM and NFM and suggest that metabolic pathways are differently regulated between FM and NFM and induce their own distinct lipidomes affecting atherosclerosis development and progression.

The levels of CEs in aortic macrophages

CEs is major component of lipid droplet in FM (31). In our lipidomic results, there were marked differences in CE species between FM and the others. The species (20:4, 18:1, 22:6, 22:4, 22:5, and 16:1) are detected in FM, but not in AM or NFM. The relative amounts of CEs were also augmented in FM (**Fig. 3D**). Gene expression related with cholesterol biosynthetic process including *Hmgcr*, *Cyp51*, *Dhcr24*, *Srebf2* and *Lbr* were downregulated in FM (**Fig. 3E**), however, FM had genes related with cholesterol esterification were increased in FM (**Fig. 3F**). *Ldlrap1*, the adaptor of LDL:LDL receptor complex in the cell membrane (32), which increased in FM. In the process of cholesterol esterification, *Npc1* and *Npc2* transported cholesterol to endoplasmic reticulum (ER) from lysosomal membrane (33), which are increased in FM. *Soat1* also increased in FM which esterified the excess cellular cholesterol to CE at the ER membrane (34). However, *Ch25h* and *Cyp27a1* are downregulated in FM, which transfer cholesterol to hydroxycholesterol. The cholesterol esterification pathway with related genes were represented in **Supplementary Fig. 5**.

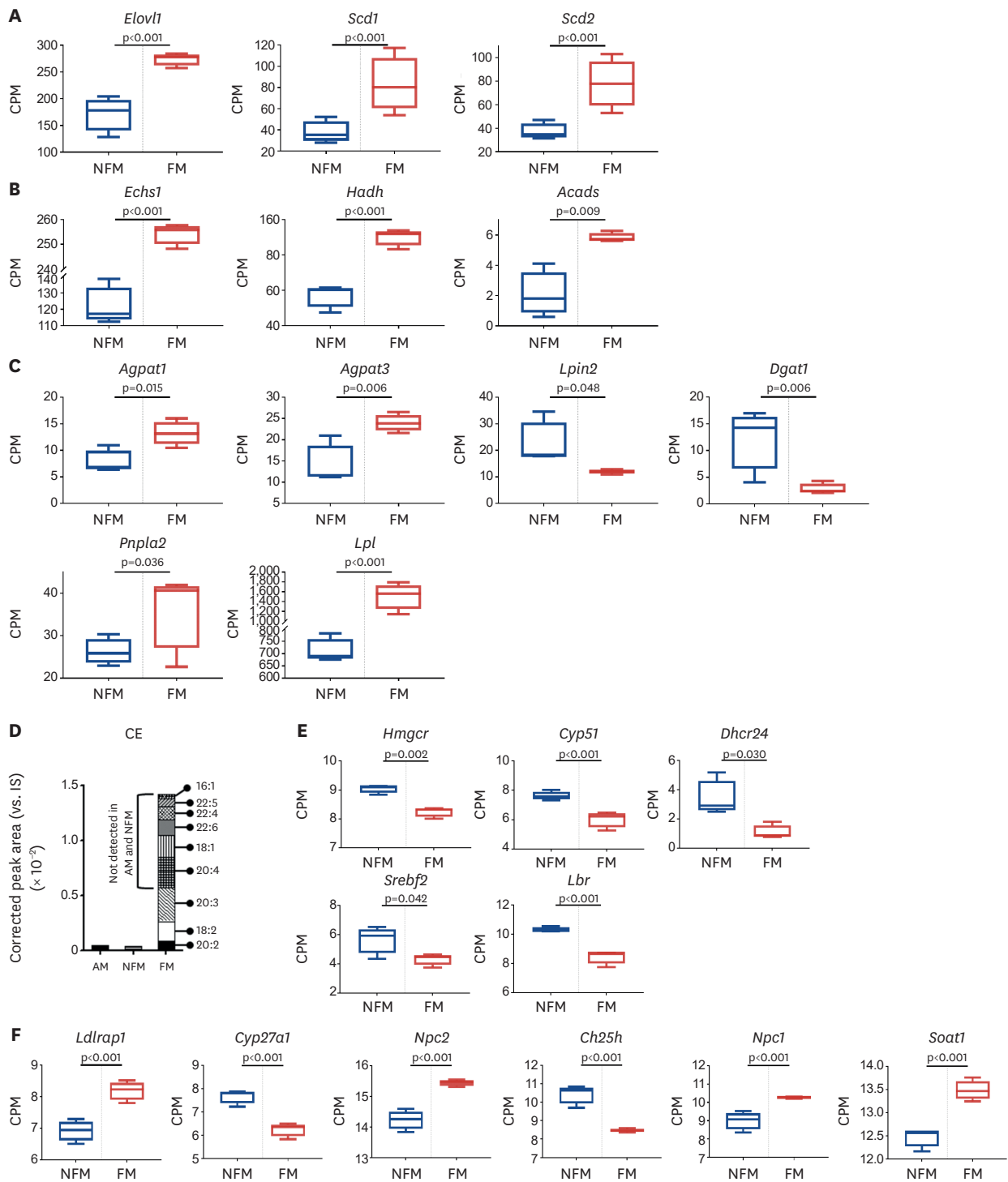


Figure 3. Differential expression of genes related to metabolic process of FA, TG and CE in intimal foamy and non-foamy macrophages. (A-C) Gene expression profile related to metabolic process of FA and TG, including *Elovl1*, *Scd1* and *Scd2* (A); *Echs1*, *Hadh*, and *Acads* (B); *Agpat1*, *Agpat3*, *Lpin2*, *Dgat1*, *Pnpla2*, and *Lpl* (C). (D) Stacked bar graphs showing the total amount of CE (relative to IS of CE) in each macrophage group. Six CE species (20:4, 18:1, 22:6, 22:4, 22:5, and 16:1) only existed in FM. (E) Box plots showing gene expression profile related to cholesterol biosynthetic process including *Hmgcr*, *Cyp51*, *Dhcr24*, *Srebf2* and *Lbr*. (F) Gene expression profile related to cholesterol esterification including *Ldlrap1*, *Ch25h*, *Cyp27a1*, *Npc1*, *Npc2* and *Soat1*. Genes of (A, B, C, E, F) were listed from bulk RNA-sequencing data (GSE116239). Differences and significance of genes between NFM and FM were determined by DEseq2 guideline (fold ratio ≥ 1.5 , $p < 0.05$).

Differential PL profiles of 3 aortic macrophage populations

Fig. 4A shows that the overall levels of some lipid classes including PC, PI, PE, and LPC in FM were higher than those in NFM. Lipid classes plotted in Fig. 4A clearly show significant increases in all classes except LPA in FM compared to NFM. Plots of the remaining 11 lipid classes are shown in Supplementary Fig. 6, with the exception in the diacylglycerol and TG.

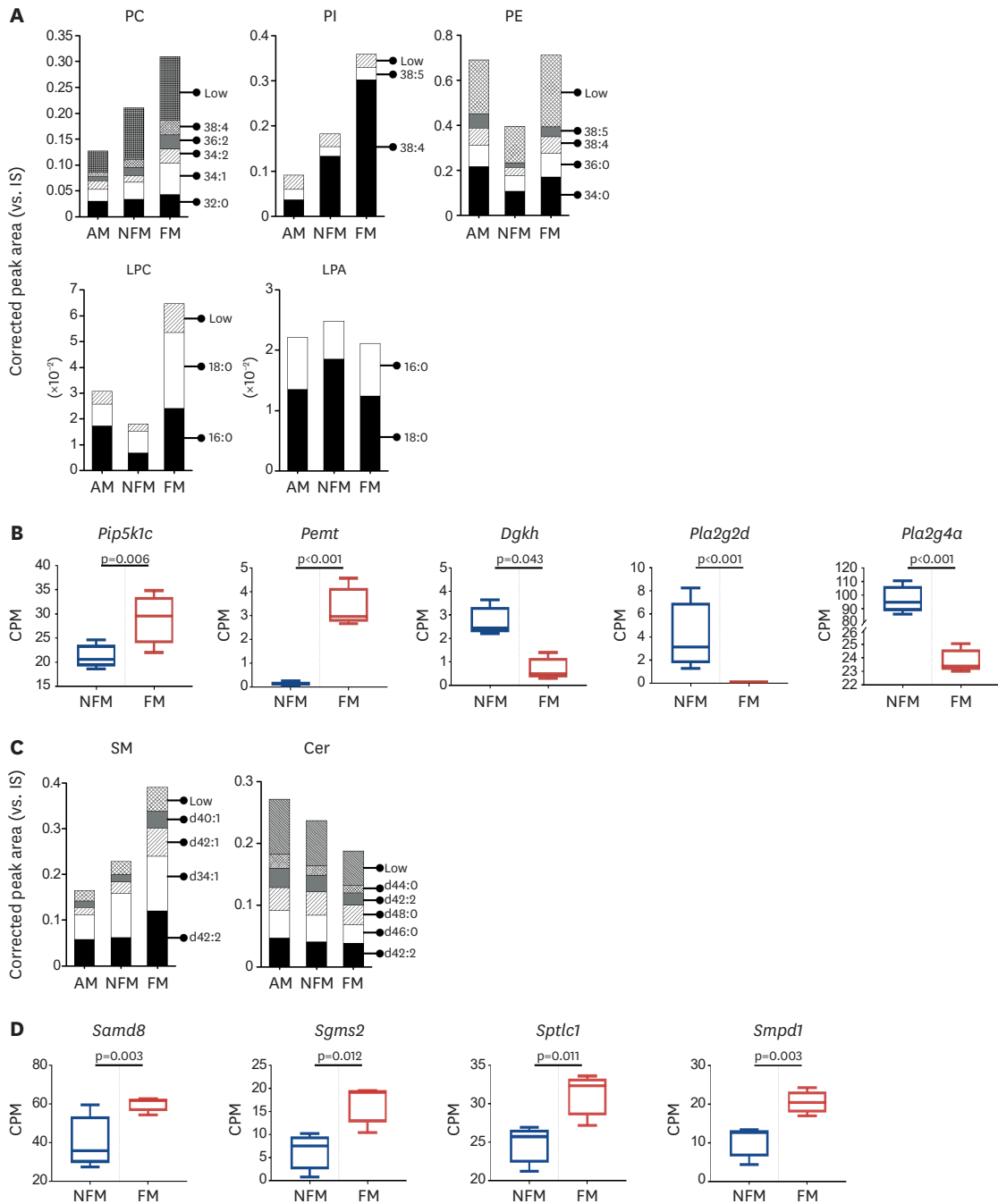


Figure 4. Differential gene expression and cellular composition of phospholipids, SM and Cer in aortic macrophages. (A) Stacked bar graphs showing the total amount of each lipid class (relative to IS specific to each lipid class) in each macrophage group. (B) Gene expression profile related to interconversion of phospholipids including *Pip5k1c*, *Pemt*, *Dgkh*, *Pla2g2d*, and *Pla2g4a*. (C) Stacked bar graphs showing the total amount of SM and Cer (relative to IS specific to each lipid class) in each macrophage group. (D) Expressions of *Samd8*, *Sgms2*, *Sptlc1* and *Smpd1* in FM and NFM. Genes were listed from bulk RNA-sequencing data (GSE116239). (B, D) Differences and significance of genes between NFM and FM were determined by DEseq2 (fold ratio ≥ 1.5 , $p < 0.05$).

The GP pathways are intertwined in a complicated manner, thus representing significant genes (**Supplementary Fig. 7A**). This shows that the bulk RNA-seq data almost coincide with those in the lipidomic analysis. For example, the level of PC is higher in FM than in others because *Pemt*, which enhances the transformation of PE to PC, is increased in FM, and *Pla2g4a*, which hydrolyzes PC to LPC, is decreased in FM (**Fig. 4B**). The overall SM level in FM was higher than that in NFM, while the overall Cer levels appeared as an opposite trend, supporting that the SM/Cer ratio was reversed in 2 intimal macrophage groups (**Fig. 4C**). Because SM is synthesized from Cer, and vice versa, the opposite trend is a reasonable result. Cer is known as an athero-prone lipid because Cer promotes the FM formation via impairing the digestion of aggregated LDL (35). Conversion between SM and Cer is represented by schematics with regulatory genes (**Supplementary Fig. 7B**). Even though both genes (*Smpd1* and *Sgms2*) used for converting SM and Cer were increased in FM, Cer may be decreased in FM because of the increased levels of *Samd8*, which catalyzes Cer to Cer phosphoethanolamine (**Fig. 4D**).

Lipid analysis of OPM

Peritoneal macrophages treated *in vitro* with oxLDL, and the untreated controls were analyzed under the same conditions employed for aortic macrophages. The quantified lipid data for the peritoneal macrophages are listed in **Supplementary Table 3**. The amounts of individual lipid species in each lipid class are plotted using stacked bar graphs in **Fig. 5A**, and the levels of PC, SM, PI, PE, and CE were found to be much higher in OPM than in CPM, as observed in the FM group. Individual TG levels are plotted using the fold ratio (OPM/CPM) in **Fig. 5B**. While the levels of ScTGs and most LcTGs in OPM were reduced to some degree or not significantly varied, the 2 TGs (52:5 and 56:5) were highly accumulated by 3-to 8-fold in the OPM group. To compare the changing patterns of each lipid class between the FM and OPM groups in comparison with the NFM and CPM groups, respectively, fold ratios of each lipid class as FM/NFM and OPM/CPM are plotted in **Fig. 5C**.

DISCUSSION

Macrophage polarization, such as M1-like and M2-like, is highly associated with the development and regression of atherosclerosis (36,37). The phenotypic conversion of macrophage is continuum and the M2 activation requires lipolysis of TG and consequent FAO, which relies on long chain FAs (22,37,38). Since mitochondrial oxidation requires TG lipolysis prior to FAO, it is known to reduce the accumulation of lipid droplets, leading to prevention of foam cell formation (39). In our experiments, the overall level of TG was not significantly changed in NFM, while it was significantly lower in FM than in adventitial cells. The comparable levels in NFM and AM were due to the decrease in the levels of most ScTGs, whereas those of most LcTGs were highly increased in NFM, offsetting each other. Most of the LcTGs showed approximately 1.5-folds higher levels in the NFM group (vs. AM), whereas those in FM were mostly reduced or not significantly changed compared to the AM group.

Among the 24 LcTG species, 2 LcTG species (52:6 and 54:2) were greatly (>2.5-fold) accumulated in both intimal macrophages compared to AM, while 3 other species (TG 56:4, 56:3, and 56:0) were largely (>2-fold) accumulated in the NFM group. In the case of peritoneal macrophages, LcTG species of the same chain lengths but with a higher degree of unsaturation (TG 52:5, 56:5, and 56:4) were observed to be largely accumulated in OPM compared to those in the control (CPM). This suggests that LcTG species with

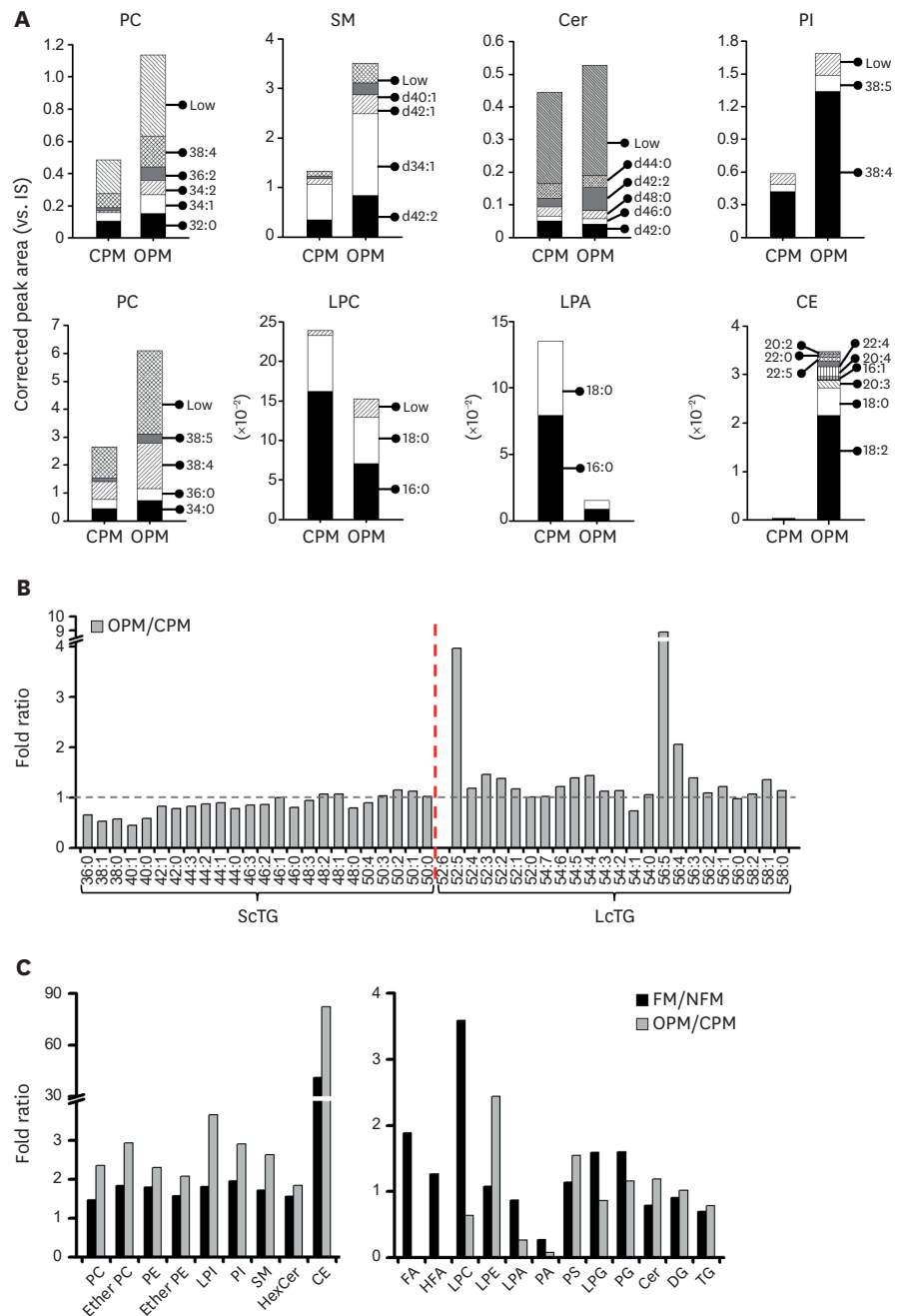


Figure 5. Lipid analysis of OPM. (A) Stacked bar graphs showing the total amount of each lipid class compared between *in vitro* cultured peritoneal macrophage groups. (B) Fold ratio of TG species in *in vitro* OPM with respect to those of CPM. Vertical dashed line refers to the point of total carbon number 50. ScTG indicates TG group with short chains, and LcTG is for TG group with long chains. (C) Fold ratio of the total amounts of each lipid class in foamy to non-foamy aortic macrophages, FM/NFM, compared with those of peritoneal macrophages treated with oxLDL to controls, OPM/CPM. LPG, lysophosphatidylglycerol; LPE, lysophosphatidylethanolamine; PA, phosphatidic acid; DG, diacylglycerol.

polyunsaturated fatty acyl chains are highly accumulated in both FM and OPM. The decreased levels of LcTG in the FM group can explain why the lipolysis of TG and the subsequent FAO of long-chain FAs in relation to the activation of the M2-like phenotype were more efficient in FM than in NFM. However, there are differences between TG species enriched in foamy

macrophages and peritoneal macrophages. Considering the difference between culture medium and *in vivo* plaque milieu, OPM appears not to perfectly represent the characteristics of foamy macrophages *in vivo*.

The levels of FA species in general were largely increased (<2-folds) in FM, along with the detection of various FA species. In particular, long polyunsaturated fatty acid species, such as FA (20:3, 20:5, 22:3, and 22:5), were exclusively found in FM, which are preferred by FAO. This evidence suggests that TG lipolysis is more favorable in FM than in NFM. FA can be taken up by macrophages through phagocytosis and the CD36 receptor, which is the receptor of both oxLDL and FA (40). The relatively upregulated expression of the CD36 gene and activated phagocytosis might contribute to the increase in FA level in FM (13,40,41). Moreover, an increased FA level is known to activate the oxidation mechanism in mitochondria because FA serves as the ligand of peroxisome proliferator-activated receptors (PPAR) (42), resulting in the M2 polarization of macrophages (36). The expression of genes related to PPAR signaling pathways was reported to be upregulated in FM (vs. NFM) in a recent study (13). It was reported that levels of FA 16:1 and 18:1 significantly increased in high-fat diet *Ldlr*^{-/-} mice compared to those of wild type (43), which is similar to the present result that both FA species increased by more than 3-folds in the FM (vs. NFM). In the case of OPM, FA and HFA were not detected, showing that TG lipolysis and subsequent oxidation of FA in relation to M2 polarization may not have been processed during the *in vitro* treatment.

Since LPC levels in oxLDLs are largely increased compared to unmodified normal LDLs, LPC levels of macrophages could be expected to be the highest in the FM and the lowest in AM (44); however, they were lowest in NFM as shown in Fig. 4A. While LPC has been widely known as pro-inflammatory lipid class, recent studies reveal its anti-inflammatory roles with dominant activities (45). Especially, the 2 LPC species (16:0 and 18:0) were reported to be associated with the increase in the efflux of cholesterol in the foam cells (45). These 2 LPC species, occupying more than 80% of total LPC amount in this study, were increased more than 3-folds in FM (vs. NFM); however, the total LPC level was even lower in NFM than AM group. In particular, LPC 18:0 has been reported to decrease pro-inflammatory cytokine level (46) and was significantly accumulated in FM group in our study. It is known that LPC not only inhibits cholesterol biosynthesis but also reduces cellular uptake of oxLDL, resulting in the attenuation of foam cell formation and atherosclerosis progression (47,48). A recent report revealed that the expression of the inflammatory gene TLR2, in which TLR-mediated signaling was inhibited by LPC, which otherwise induces M1 polarization in macrophages, was suppressed in FM but elevated in NFM (13), which is consistent with our LPC data. In the case of OPM, the LPC level was lower than that in the CPM group, which is similar to the decreasing pattern of LPC in NFM compared with that in AM. Based on this evidence, NFM, which has the lowest levels of LPC among the 3 groups, seems to be less anti-inflammatory than FM.

In summary, this study introduced a comprehensive lipidomic analysis of 3 different types of aortic macrophages extracted from mice with hyperlipidemia using nUHPLC-ESI-MS/MS (Fig. 6). TG species with long fatty acyl chains showed different patterns in FM and NFM, while the level of their lipolysis product, FA, was the highest in FM. Lipid classes, including CE, SM, and PC, which are positively associated with the uptake of LDLs, were highly accumulated in intimal macrophages, with higher levels in FM. Levels of PE, LPC, and AA containing lipid species were lower in NFM when compared between the 2 intimal macrophages. As a result, we observed different levels of lipid species closely related to

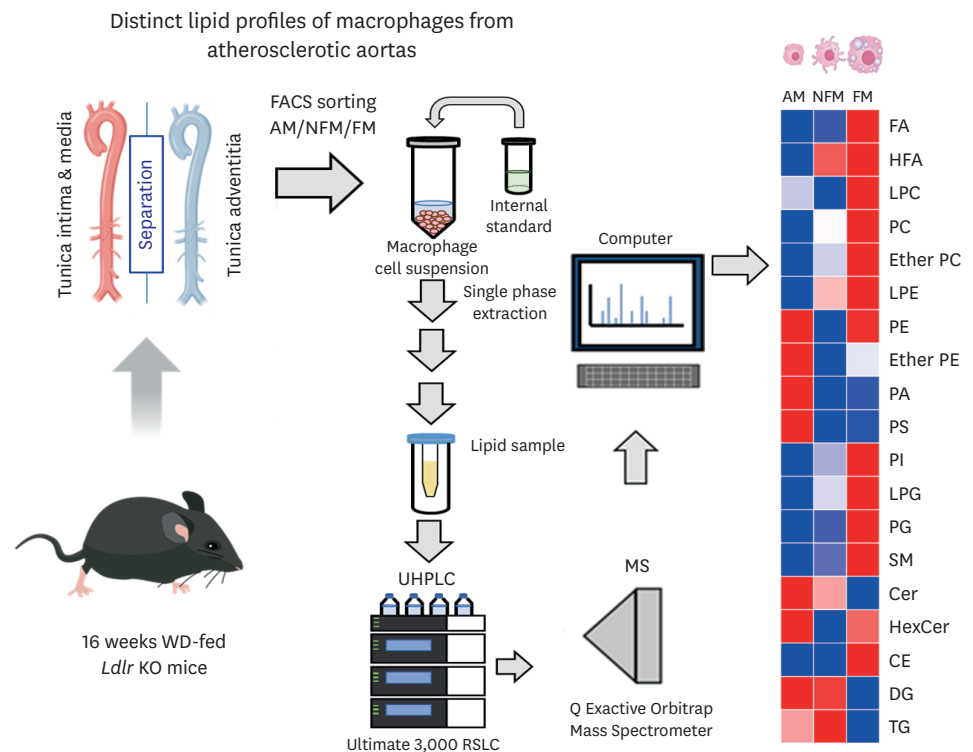


Figure 6. Schematic diagram representing the lipid species in aortic macrophages. The abundance and heterogeneity of lipid species in FM, NFM, and AM isolated from murine atherosclerotic aorta demonstrated that each macrophage population has a distinct proportion of lipid species. WD, Western diet; KO, knockout; LPE, lysophosphatidylethanolamine; PA, phosphatidic acid; PG, phosphatidylglycerol; LPG, lysophosphatidylglycerol.

atherosclerosis or inflammation in each group of macrophages, which could provide strong evidence for the transcriptomic outcome that NFM rather than FM are pro-inflammatory in atherosclerosis (13). Our results appear to be helpful to understand the phenotypic changes of macrophages during hyperlipidemic condition and to address unsolved questions related to the development and regression of atherosclerosis.

However, there are several issues that need to be elucidated by further study. Firstly, it is necessary to define the specific lipid mediators responsible for the less inflammatory phenotype of FM. Previously, it has been shown that lipid-laden macrophages exhibit down-regulated expression of genes related to inflammation through the activation of the liver X receptor pathway by desmosterol. Additionally, increased FAs may induce anti-inflammatory programming via activation of PPAR γ . Therefore, further investigation is needed to identify and analyze the lipid species present in foam cells and evaluate their effects on the phenotypic changes of macrophages. Secondly, the lipidomics analysis in this study was based on repeated measurements of a single lipid extract, which only demonstrates technical reproducibility. Although we observed a strong correlation between the enriched lipid species in FM and gene expression related to lipid production, it is necessary to conduct targeted lipid analysis for FAs, eicosanoids, and docosanoids. This analysis will not only confirm the differential levels of FAs among macrophages but also identify more precise lipid mediators responsible for the cellular phenotype of foam cells. Lastly, it is crucial to perform lipidomics analysis on foam cells and non-foam cells sorted from human atherosclerotic plaques and compare the results with the murine data. Since the duration of atherosclerotic

lesion formation differs significantly between humans and mouse models, the lipid species accumulated in foam cells may vary, and their metabolic processes may differ as well.

ACKNOWLEDGEMENTS

This work was supported by the National Research Foundation (NRF) of Korea (NRF-2021R1A2C2003171, 2021R1A2C3004586, RS-2023-00207840, and 2016M3A9D5A01952413).

SUPPLEMENTARY MATERIALS

Supplementary Data 1

Supplemental methods and materials

[Click here to view](#)

Supplementary Table 1

Number of identified/quantified lipid species in each lipid class

[Click here to view](#)

Supplementary Table 2

List of identified lipids along with isomeric chain structures

[Click here to view](#)

Supplementary Table 3

Fold ratio of each lipid species in NFM compared to AM (NFM/AM), FM compared to AM (FM/AM), and to NFM (FM/NFM), and OPM/CPM

[Click here to view](#)

Supplementary Table 4

Type of precursor and quantifier ions of each lipid class and the list of IS used for each lipid class

[Click here to view](#)

Supplementary Table 5

Concentration of FA species in the blank injections

[Click here to view](#)

Supplementary Table 6

List of TGs containing each corresponding FA as acyl chain

[Click here to view](#)

Supplementary Table 7

Experimental MS parameters for nUHPLC-ESI-MS/MS analysis

[Click here to view](#)

Supplementary Figure 1

BPCs of lipid standards in (A) positive and (B) negative ion mode of nUHPLC-ESI-MS/MS. The analysis was repeated 6 times in total with 3 times in positive and negative ion modes respectively.

[Click here to view](#)

Supplementary Figure 2

BPCs of lipid extracts from the three different macrophage groups in (A) positive and (B) negative ion modes of nUHPLC-ESI-MS/MS. The analysis was repeated 6 times (3 times in positive and negative ion modes respectively) for the identification of lipid species with the amount of lipid extract equivalent to 200 cells were injected each run.

[Click here to view](#)

Supplementary Figure 3

Corrected peak area of FAs that were not included in **Fig. 2C**. Student's t-test was utilized to analyze the differences of total levels of FA between the two macrophage populations.

[Click here to view](#)

Supplementary Figure 4

Schematics of FA biosynthetic process, FA beta-oxidation and TG metabolism with related genes. The red color indicates the upregulated genes in FM, and the blue indicates the downregulated genes in FM.

[Click here to view](#)

Supplementary Figure 5

The schematics represent cholesterol biosynthetic process and esterification pathway with related genes. The red color indicates the upregulated genes in FM than NFM, and the blue indicates the downregulated genes in FM.

[Click here to view](#)

Supplementary Figure 6

Stacked bar graphs showing the total amount of each lipid class that are not shown in main figures.

[Click here to view](#)

Supplementary Figure 7

(A) The schematics represent conversion between phospholipids with its related genes. The red color indicates the upregulated genes in FM than NFM and the blue indicates the

downregulated genes in FM. (B) Schematics represent the conversion of SM and Cer with related genes. The red color indicates the upregulated genes in FM.

[Click here to view](#)

REFERENCES

1. VanderLaan PA, Reardon CA, Getz GS. Site specificity of atherosclerosis: site-selective responses to atherosclerotic modulators. *Arterioscler Thromb Vasc Biol* 2004;24:12-22.
[PUBMED](#) | [CROSSREF](#)
2. Zhang S, Ritter LR, Ibragimov AI. Foam cell formation in atherosclerosis: HDL and macrophage reverse cholesterol transport. *Conf Publ* 2013;2013:825-835.
[CROSSREF](#)
3. Cole JE, Park I, Ahern DJ, Kassiteridi C, Danso Abeam D, Goddard ME, Green P, Maffia P, Monaco C. Immune cell census in murine atherosclerosis: cytometry by time of flight illuminates vascular myeloid cell diversity. *Cardiovasc Res* 2018;114:1360-1371.
[PUBMED](#) | [CROSSREF](#)
4. Glass CK, Witztum JL. Atherosclerosis. The road ahead. *Cell* 2001;104:503-516.
[PUBMED](#) | [CROSSREF](#)
5. Fahy E, Subramaniam S, Brown HA, Glass CK, Merrill AH Jr, Murphy RC, Raetz CR, Russell DW, Seyama Y, Shaw W, et al. A comprehensive classification system for lipids. *J Lipid Res* 2005;46:839-861.
[PUBMED](#) | [CROSSREF](#)
6. Brouwers JF, Vernooij EA, Tielens AG, van Golde LM. Rapid separation and identification of phosphatidylethanolamine molecular species. *J Lipid Res* 1999;40:164-169.
[PUBMED](#) | [CROSSREF](#)
7. Wenk MR. The emerging field of lipidomics. *Nat Rev Drug Discov* 2005;4:594-610.
[PUBMED](#) | [CROSSREF](#)
8. Stegemann C, Drozdov I, Shalhoub J, Humphries J, Ladroue C, Didangelos A, Baumert M, Allen M, Davies AH, Monaco C, et al. Comparative lipidomics profiling of human atherosclerotic plaques. *Circ Cardiovasc Genet* 2011;4:232-242.
[PUBMED](#) | [CROSSREF](#)
9. Wilson PW, Kannel WB. Obesity, diabetes, and risk of cardiovascular disease in the elderly. *Am J Geriatr Cardiol* 2002;11:119-124.
[PUBMED](#) | [CROSSREF](#)
10. Santos CR, Schulze A. Lipid metabolism in cancer. *FEBS J* 2012;279:2610-2623.
[PUBMED](#) | [CROSSREF](#)
11. Lee GB, Lee JC, Moon MH. Plasma lipid profile comparison of five different cancers by nanoflow ultrahigh performance liquid chromatography-tandem mass spectrometry. *Anal Chim Acta* 2019;1063:117-126.
[PUBMED](#) | [CROSSREF](#)
12. Remmerie A, Scott CL. Macrophages and lipid metabolism. *Cell Immunol* 2018;330:27-42.
[PUBMED](#) | [CROSSREF](#)
13. Kim K, Shim D, Lee JS, Zaitsev K, Williams JW, Kim KW, Jang MY, Seok Jang H, Yun TJ, Lee SH, et al. Transcriptome analysis reveals nonfoamy rather than foamy plaque macrophages are proinflammatory in atherosclerotic murine models. *Circ Res* 2018;123:1127-1142.
[PUBMED](#) | [CROSSREF](#)
14. Zhang C, Wang Y, Wang F, Wang Z, Lu Y, Xu Y, Wang K, Shen H, Yang P, Li S, et al. Quantitative profiling of glycerophospholipids during mouse and human macrophage differentiation using targeted mass spectrometry. *Sci Rep* 2017;7:412.
[PUBMED](#) | [CROSSREF](#)
15. Hsieh WY, Zhou QD, York AG, Williams KJ, Scumpia PO, Kronenberger EB, Hoi XP, Su B, Chi X, Bui VL, et al. Toll-like receptors induce signal-specific reprogramming of the macrophage lipidome. *Cell Metab* 2020;32:128-143.e5.
[PUBMED](#) | [CROSSREF](#)
16. Paul A, Lydic TA, Hogan R, Goo YH. Cholesterol acceptors regulate the lipidome of macrophage foam cells. *Int J Mol Sci* 2019;20:3784.
[PUBMED](#) | [CROSSREF](#)

17. Martin M. Cutadapt removes adapter sequences from high-throughput sequencing reads. *EMBnet J* 2019;17:10-12.
[CROSSREF](#)
18. Dobin A, Davis CA, Schlesinger F, Drenkow J, Zaleski C, Jha S, Batut P, Chaisson M, Gingeras TR. STAR: ultrafast universal RNA-seq aligner. *Bioinformatics* 2013;29:15-21.
[PUBMED](#) | [CROSSREF](#)
19. Anders S, Pyl PT, Huber W. HTSeq--a Python framework to work with high-throughput sequencing data. *Bioinformatics* 2015;31:166-169.
[PUBMED](#) | [CROSSREF](#)
20. Love MI, Huber W, Anders S. Moderated estimation of fold change and dispersion for RNA-seq data with DESeq2. *Genome Biol* 2014;15:550.
[PUBMED](#) | [CROSSREF](#)
21. Wang L, Wang S, Li W. RSeQC: quality control of RNA-seq experiments. *Bioinformatics* 2012;28:2184-2185.
[PUBMED](#) | [CROSSREF](#)
22. Castoldi A, Monteiro LB, van Teijlingen Bakker N, Sanin DE, Rana N, Corrado M, Cameron AM, Hässler F, Matsushita M, Caputa G, et al. Triacylglycerol synthesis enhances macrophage inflammatory function. *Nat Commun* 2020;11:4107.
[PUBMED](#) | [CROSSREF](#)
23. Lone AM, Taskén K. Proinflammatory and immunoregulatory roles of eicosanoids in T cells. *Front Immunol* 2013;4:130.
[PUBMED](#) | [CROSSREF](#)
24. Meikle PJ, Wong G, Tsorotes D, Barlow CK, Weir JM, Christopher MJ, MacIntosh GL, Goudey B, Stern L, Kowalczyk A, et al. Plasma lipidomic analysis of stable and unstable coronary artery disease. *Arterioscler Thromb Vasc Biol* 2011;31:2723-2732.
[PUBMED](#) | [CROSSREF](#)
25. Tallima H, El Ridi R. Arachidonic acid: physiological roles and potential health benefits - a review. *J Adv Res* 2017;11:33-41.
[PUBMED](#) | [CROSSREF](#)
26. Xu M, Wang X, Li Y, Geng X, Jia X, Zhang L, Yang H. Arachidonic acid metabolism controls macrophage alternative activation through regulating oxidative phosphorylation in PPAR γ dependent manner. *Front Immunol* 2021;12:618501.
[PUBMED](#) | [CROSSREF](#)
27. Gaudet P, Livstone MS, Lewis SE, Thomas PD. Phylogenetic-based propagation of functional annotations within the Gene Ontology consortium. *Brief Bioinform* 2011;12:449-462.
[PUBMED](#) | [CROSSREF](#)
28. Ishimoto K, Nakamura H, Tachibana K, Yamasaki D, Ota A, Hirano KI, Tanaka T, Hamakubo T, Sakai J, Kodama T, et al. Sterol-mediated regulation of human lipin 1 gene expression in hepatoblastoma cells. *J Biol Chem* 2009;284:22195-22205.
[PUBMED](#) | [CROSSREF](#)
29. Eichmann TO, Kumari M, Haas JT, Farese RV Jr, Zimmermann R, Lass A, Zechner R. Studies on the substrate and stereo/regioselectivity of adipose triglyceride lipase, hormone-sensitive lipase, and diacylglycerol-O-acyltransferases. *J Biol Chem* 2012;287:41446-41457.
[PUBMED](#) | [CROSSREF](#)
30. Fruchart-Najib J, Baugé E, Niculescu LS, Pham T, Thomas B, Rommens C, Majd Z, Brewer B, Pennacchio LA, Fruchart JC. Mechanism of triglyceride lowering in mice expressing human apolipoprotein A5. *Biochem Biophys Res Commun* 2004;319:397-404.
[PUBMED](#) | [CROSSREF](#)
31. Brown MS, Ho YK, Goldstein JL. The cholesteryl ester cycle in macrophage foam cells. Continual hydrolysis and re-esterification of cytoplasmic cholesteryl esters. *J Biol Chem* 1980;255:9344-9352.
[PUBMED](#) | [CROSSREF](#)
32. Garuti R, Jones C, Li WP, Michaely P, Herz J, Gerard RD, Cohen JC, Hobbs HH. The modular adaptor protein autosomal recessive hypercholesterolemia (ARH) promotes low density lipoprotein receptor clustering into clathrin-coated pits. *J Biol Chem* 2005;280:40996-41004.
[PUBMED](#) | [CROSSREF](#)
33. Liou HL, Dixit SS, Xu S, Tint GS, Stock AM, Lobel P. NPC2, the protein deficient in Niemann-Pick C2 disease, consists of multiple glycoforms that bind a variety of sterols. *J Biol Chem* 2006;281:36710-36723.
[PUBMED](#) | [CROSSREF](#)
34. Cadigan KM, Heider JG, Chang TY. Isolation and characterization of Chinese hamster ovary cell mutants deficient in acyl-coenzyme A:cholesterol acyltransferase activity. *J Biol Chem* 1988;263:274-282.
[PUBMED](#) | [CROSSREF](#)

35. Shu H, Peng Y, Hang W, Li N, Zhou N, Wang DW. Emerging roles of ceramide in cardiovascular diseases. *Aging Dis* 2022;13:232-245.
[PUBMED](#) | [CROSSREF](#)
36. Leitinger N, Schulman IG. Phenotypic polarization of macrophages in atherosclerosis. *Arterioscler Thromb Vasc Biol* 2013;33:1120-1126.
[PUBMED](#) | [CROSSREF](#)
37. Bi Y, Chen J, Hu F, Liu J, Li M, Zhao L. M2 macrophages as a potential target for antiatherosclerosis treatment. *Neural Plast* 2019;2019:6724903.
[PUBMED](#) | [CROSSREF](#)
38. Huang SC, Everts B, Ivanova Y, O'Sullivan D, Nascimento M, Smith AM, Beatty W, Love-Gregory L, Lam WY, O'Neill CM, et al. Cell-intrinsic lysosomal lipolysis is essential for alternative activation of macrophages. *Nat Immunol* 2014;15:846-855.
[PUBMED](#) | [CROSSREF](#)
39. Genoula M, Marín Franco JL, Maio M, Dolotowicz B, Ferreyra M, Milillo MA, Mascarau R, Moraña EJ, Palmero D, Matteo M, et al. Fatty acid oxidation of alternatively activated macrophages prevents foam cell formation, but *Mycobacterium tuberculosis* counteracts this process via HIF-1 α activation. *PLoS Pathog* 2020;16:e1008929.
[PUBMED](#) | [CROSSREF](#)
40. Yu XH, Fu YC, Zhang DW, Yin K, Tang CK. Foam cells in atherosclerosis. *Clin Chim Acta* 2013;424:245-252.
[PUBMED](#) | [CROSSREF](#)
41. Ménégaut L, Jalil A, Thomas C, Masson D. Macrophage fatty acid metabolism and atherosclerosis: the rise of PUFAs. *Atherosclerosis* 2019;291:52-61.
[PUBMED](#) | [CROSSREF](#)
42. Grygiel-Górniak B. Peroxisome proliferator-activated receptors and their ligands: nutritional and clinical implications--a review. *Nutr J* 2014;13:17.
[PUBMED](#) | [CROSSREF](#)
43. Spann NJ, Garmire LX, McDonald JG, Myers DS, Milne SB, Shibata N, Reichart D, Fox JN, Shaked I, Heudobler D, et al. Regulated accumulation of desmosterol integrates macrophage lipid metabolism and inflammatory responses. *Cell* 2012;151:138-152.
[PUBMED](#) | [CROSSREF](#)
44. Orsó E, Matysik S, Grandl M, Liebisch G, Schmitz G. Human native, enzymatically modified and oxidized low density lipoproteins show different lipidomic pattern. *Biochim Biophys Acta* 2015;1851:299-306.
[PUBMED](#) | [CROSSREF](#)
45. Knuplez E, Marsche G. An updated review of pro- and anti-inflammatory properties of plasma lysophosphatidylcholines in the vascular system. *Int J Mol Sci* 2020;21:4501.
[PUBMED](#) | [CROSSREF](#)
46. Maciel E, Felgueiras J, Silva EM, Ricardo F, Moreira AS, Melo T, Campos A, Fardilha M, Domingues P, Domingues MR. Lipid remodelling in human melanoma cells in response to UVA exposure. *Photochem Photobiol Sci* 2017;16:744-752.
[PUBMED](#) | [CROSSREF](#)
47. Rosenblat M, Oren R, Aviram M. Lysophosphatidylcholine (LPC) attenuates macrophage-mediated oxidation of LDL. *Biochem Biophys Res Commun* 2006;344:1271-1277.
[PUBMED](#) | [CROSSREF](#)
48. Schmitz G, Ruebsaamen K. Metabolism and atherogenic disease association of lysophosphatidylcholine. *Atherosclerosis* 2010;208:10-18.
[PUBMED](#) | [CROSSREF](#)